

Iron nanoparticles decorated graphene-multiwalled carbon nanotubes nanocomposite-modified glassy carbon electrode for the sensitive determination of nitrite

Veerappan Mani · Tzu-Ying Wu · Shen-Ming Chen

Received: 20 September 2013 / Revised: 25 November 2013 / Accepted: 29 November 2013 / Published online: 14 December 2013
© Springer-Verlag Berlin Heidelberg 2013

Abstract In the present work, we described the preparation of iron nanoparticles decorated graphene-multiwalled carbon nanotubes nanocomposite (GR-MWCNTs/FeNPs) modified glassy carbon electrode (GCE) and its application for the sensitive determination of nitrite. First, GR-MWCNTs/FeNPs nanocomposite has been prepared by a simple solution-based approach via chemical reduction and then it was characterized. Afterwards, GR-MWCNTs/FeNPs/GCE was prepared and employed for the electrocatalysis of nitrite. Electrocatalytic oxidation of nitrite at the GR-MWCNTs/FeNPs/GCE has been significantly improved in terms of both reduction in overpotential and increase in peak current. Therefore, the modified electrode was employed for amperometric determination of nitrite which exhibited excellent analytical parameters with wide linear range of 1×10^{-7} M to 1.68×10^{-3} M and very low detection limit of 75.6 (± 1.3) nM. The proposed sensor selectively detects nitrite even in the presence of high concentration of common ions and biological interferences. Good recoveries achieved for the determination of nitrite in various water samples reveal the promising practicality of the sensor. In addition, the sensor displays an acceptable repeatability and reproducibility along with appreciable storage and excellent operational stabilities.

Keywords Graphene · Carbon nanotube · Iron nanoparticles · Nitrite · Electrocatalysis · Amperometry

Introduction

Graphene (GR), the thinnest known material in the universe is a well-known allotrope of carbon composed of sp^2 hybridized carbon atoms with planar structure [1–3]. Graphene-based research becomes viral throughout the entire research world after its successful preparation via simple scotch tape method [3]. Chemical oxidation and subsequent reduction of graphite is one of the desirable routes to prepare scalable quantity of graphene [2]. Similarly, carbon nanotubes (CNTs), another well-known allotrope of carbon, dominated the whole material science research since its discovery in 1991, ascribed to its outstanding physicochemical properties [4]. Notably, production of graphene is via cheaper chemical oxidation–reduction approach, while production of CNTs is usually via expensive chemical vapor deposition approach [5]. In contrast, processability of both graphene and CNTs is the key challenge since their individual dispersions in organic solvents lead to irreversible agglomeration and limit their applications.

Recently several approaches were made to prepare GR-CNTs hybrid aiming to collectively assemble the unique properties of these two important carbon allotropes [6, 7]. Integrating GR and CNTs (both single walled carbon nanotubes or multiwalled carbon nanotubes (MWCNTs)) as hybrid presume strong synergy; as a result, the hybrid can offer superior performances than either pristine GR or CNTs. Due to the exceptional properties of GR-CNTs, it finds extensive applications in diverse research fields including supercapacitors [8], dye-sensitized solar cells (DSSC) [9], sensors [10], biosensors [11], and biofuel cells [12]. Structurally, GR-CNTs hybrid can be viewed as three-dimensional hierarchical assembling of two dimensional GR sheets and one-dimensional CNTs through π – π stacking interaction [11]. CNTs act as conducting wires or spacers between GR sheets which helps to inhibit the stacking of sheets. Studies proved that GR-CNTs hybrid exhibited higher electrical conductivities, large specific

V. Mani · T.-Y. Wu · S.-M. Chen (✉)
Electroanalysis and Bioelectrochemistry Lab, Department of
Chemical Engineering and Biotechnology, National Taipei
University of Technology, No. 1, Section 3, Chung-Hsiao East Road,
Taipei 106, Taiwan, People's Republic of China
e-mail: smchen78@ms15.hinet.net

area, and superior catalytic properties over pristine CNTs and GR [10, 11, 13]. Most reports claimed that a great synergic effect was operating between GR and CNTs, which is responsible for the improved performance of GR-CNTs hybrid [7, 11]. On the other hand, Buglione and Pumera [14] showed that the improved performance of the hybrid is due to the arithmetic average of weight-specific capacitance of GR and CNTs. Notably, Stoner and Glass revealed that GR-CNTs hybrid is able to provide the highest edge density than any other carbon nanostructures [13]. In this view point, we previously reported the greatly enhanced electrocatalytic performance of GR-CNTs hybrid towards sensor [10] and biosensor [11] applications. Wang et al. fabricated efficient supercapacitors and achieved appreciably improved performances by make use of GR-CNTs hybrid [15]. DSSC performance was significantly enhanced in terms of greater degree of dye adsorption and reduction in charge of recombination process when GR-CNTs hybrid was employed as photo anodes [9]. Thus, GR-CNTs hybrid is a unique nanostructured material with superior abilities than either GR or CNTs.

In the past years, several efforts were developed to make use of CNTs and GR as support materials to anchor metal nanoparticles [16, 17]. In this way, it is very attractive to employ GR-CNTs hybrid as a mat to anchor metal nanoparticles due to the abovementioned excellent abilities and performances of the hybrid [18]. Hence, in the present work, we utilized GR-CNTs hybrid as a catalyst mat to support iron nanoparticles, which in turn, is a good electrocatalyst to oxidize nitrite [19]. Moreover, decoration of Fe nanoparticles (FeNPs) contributes to the stability of the hybrid by acting as spacers between the sheets and tubes. Notably, here, we employed a single-step chemical reduction process for the simultaneous reduction of iron precursor to iron nanoparticles and graphene oxide (GO) to graphene.

Determination of nitrite (NO_2^-) in various food products, drinking water, and animal feeds are highly important for the welfare of both human and livestock [20]. Owing to the advantages of electrochemical techniques, great deals of attention were made for the electrochemical determination of nitrite in the past years [21–25]. Some of the recently reported electrochemical nitrite sensors includes gold nanoparticles and sulfonated graphene composite [20], Single-layer reduced graphene oxide-multiwalled carbon nanotubes [21], bare glassy carbon electrode [22], graphene/polypyrrole/chitosan nanocomposite [23], chemically reduced graphene oxide [24], and thionine-modified aligned CNTs [25]. In this way, herein we explored a sensitive amperometric sensor at graphene-multiwalled carbon nanotubes/iron nanoparticles (GR-MWCNTs/FeNPs) modified electrode. The superior electrocatalytic ability of the iron nanoparticles decorated GR-MWCNTs hybrid has been revealed with achievement of excellent analytical parameters with very low detection limit of 75.6 (± 1.3) nM.

Experimental

Reagents and apparatus

Graphite (powder $<20 \mu\text{m}$), MWCNTs (bundled $>95 \%$), ferric chloride (FeCl_3), sodium borohydride (NaBH_4), sodium nitrite, and all other chemicals were purchased from Sigma-Aldrich. All the reagents used were of analytical grade and used as received. Supporting electrolyte used for the electrochemical studies was 0.05-M phosphate buffer solution (PBS), prepared using Na_2HPO_4 and NaH_2PO_4 and the required pH solution was adjusted either using H_2SO_4 or NaOH . Pure double distilled water (conductivity $\geq 18 \text{ M}\Omega$) was utilized for all the experiments.

Electrochemical measurements were carried out using CHI 1205A work station with a conventional three electrode cell using BAS GCE as the working electrode (area 0.071 cm^2), saturated Ag/AgCl as the reference electrode, and Pt wire as the counter electrode. Amperometric measurements were performed with analytical rotator AFMSRX (Pine instruments, USA) with a rotating disk electrode. Scanning electron microscopy (SEM) and energy-dispersive x-ray (EDX) spectra studies were carried out in Hitachi S-3000H scanning electron microscope and HORIBA EMAX X-ACT (Model 51-ADD0009, Sensor + 24 V=16 W, resolution at 5.9 keV), respectively. Transmission electron microscopy (TEM) and powder x-ray diffraction (XRD) studies were performed in Hitachi H-7000 and X'PERT-PRO (PANalytical B.V., The Netherlands) diffractometer using $\text{Cu K}\alpha$ radiation ($k=1.54 \text{ \AA}$). EIM6ex ZAHNER (Kroanch, Germany) was used for electrochemical impedance spectroscopy (EIS) studies.

Preparation of GR-MWCNTs/FeNPs nanocomposite-modified GCE

Graphite oxide was prepared from graphite by modified Hummer's method [26] and exfoliated to GO via ultrasonication for 1 h and subsequently centrifuged (4,000 RPM) for 30 min to remove unexfoliated graphite oxide. MWCNTs were added to the GO dispersion and the resulting mixture was ultrasonicated for 2 h to get GO-MWCNTs hybrid. Thus obtained GO-MWCNTs hybrid was separated, washed, dried, and redispersed in water (1 mg mL^{-1}). Then, FeCl_3 solution (1 mg mL^{-1}) was added into GO-MWCNTs hybrid and the resulting mixture was stirred for 30 min. NaBH_4 was slowly added to the above mixture with constant stirring and the entire mixture was kept stirred for 3 h. Addition of NaBH_4 resulting in simultaneous reduction of ferric ion into FeNPs and GO into graphene. Upon completion of reduction, the reaction mixture was filtered and washed with ethanol and water, respectively. The as-purified GR-MWCNTs/FeNPs nanocomposite was dried overnight and redispersed (0.5 mg mL^{-1}) in ethanol. Schematic

representation of the preparation of GR-MWCNTs/FeNPs nanocomposite has been given in Scheme 1.

GCE surface was polished with alumina slurry using a Buehler polishing kit and subsequently ultrasonicated in ethanol and water for 5 min and dried. Six microliters of GR-MWCNTs/FeNPs nanocomposite was drop casted onto the pre-cleaned GCE and dried at room temperature. Afterwards, GR-MWCNTs/FeNPs nanocomposite-modified GCE (GR-MWCNTs/FeNPs/GCE) was rinsed with water and used for all the experiments. For comparison, GR-MWCNTs and unmodified GCEs were prepared by adopting similar procedures.

Results and discussions

Characterization of the as-prepared composite

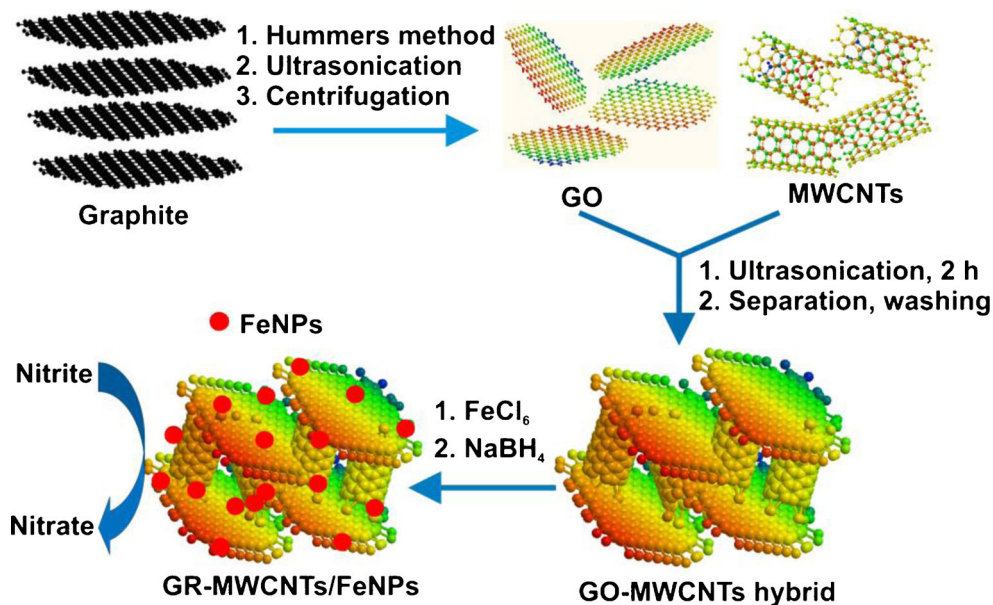
SEM image of graphene (Fig. 1a) represents the typical sheet like morphology with foldings and crumbles over the sheets. EDX spectrum of graphene (Fig. 1b) shows signals for the presence of carbon and oxygen with weight percentages 89.54 and 10.46 %, respectively. EDX spectra were carried out on indium tin oxide (ITO) surface and the EDX signals corresponding to ITO were omitted for the sake of clarification. SEM (Fig. 1c) of GR-CNTs hybrid portrays with wrinkled GR sheets wrapped around the tubular networks of MWCNTs. As we reported earlier, there might be a non-covalent π - π stacking interaction operating between GR sheets and CNTs [10, 11]. EDX spectrum of GR-MWCNTs (Fig. 1d) hybrid exhibited signals for carbon and oxygen with weight percentages 89.85 and 10.15 %.

SEM (Fig. 1e) of GR-MWCNTs/FeNPs nanocomposite shows the characteristic morphology of GR-MWCNTs hybrid

along with decoration of iron nanoparticles with size ranging in nanometers. The residual oxygenated functional groups present on the GR surface act as active sites for the growth of FeNPs. EDX of GR-MWCNTs/FeNPs nanocomposite (Fig. 1f) shows the presence of signals for C, O, and Fe with weight percentages 79.25, 8.59, and 12.16 %, respectively. Obviously, the existence of Fe signals shows the presence of FeNPs and confirms the firm attachment of FeNPs to the GR-MWCNTs hybrid. Notably, the observed small percent of oxygen stands for the presence of unreduced oxygen functional groups resided on the graphene sheets. TEM of GR (Fig. 2a) shows the characteristic sheet like morphology of graphene with thickness of the sheets varies from 2 to 3 nm. In the TEM of GR-MWCNTs (Fig. 2b), tubular networks of MWCNTs were entrapped and covered by the GR sheets which ultimately prevent the aggregation of MWCNTs. TEM of GR-MWCNTs/FeNPs nanocomposite (Fig. 2c) revealed the decoration of FeNPs onto the sheets of GR and tip of MWCNTs with the particle sizes ranging from 20 to 30 nm. Thus, TEM results as well confirmed the formation of GR-MWCNTs hybrid and GR-MWCNTs/FeNPs nanocomposite.

Figure 3a demonstrates the impedance spectra represented as Nyquist plots of bare, GR-MWCNTs and GR-MWCNTs/FeNPs nanocomposite-modified GCEs in PBS (pH 7) containing 5-mM $\text{Fe}(\text{CN})_6^{3-/4-}$. Randles equivalent circuit model used to fit the experimental data is given as inset to Fig. 3a, where, R_{ct} is charge transfer resistance, R_s is electrolyte resistance, C_{dl} is double layer capacitance, and Z_w is Warburg impedance. EIS experiments were carried out at a bias potential of 0 V with amplitude of 5 mV. Compared with bare GCE, GR-MWCNTs/GCE exhibited a semicircle of small diameter ascribed to the significant decrease in electrical resistance after modification with hybrid which revealed the excellent

Scheme 1 Schematic representation for the preparation of GR-MWCNTs/FeNPs nanocomposite and its electrocatalysis towards nitrite



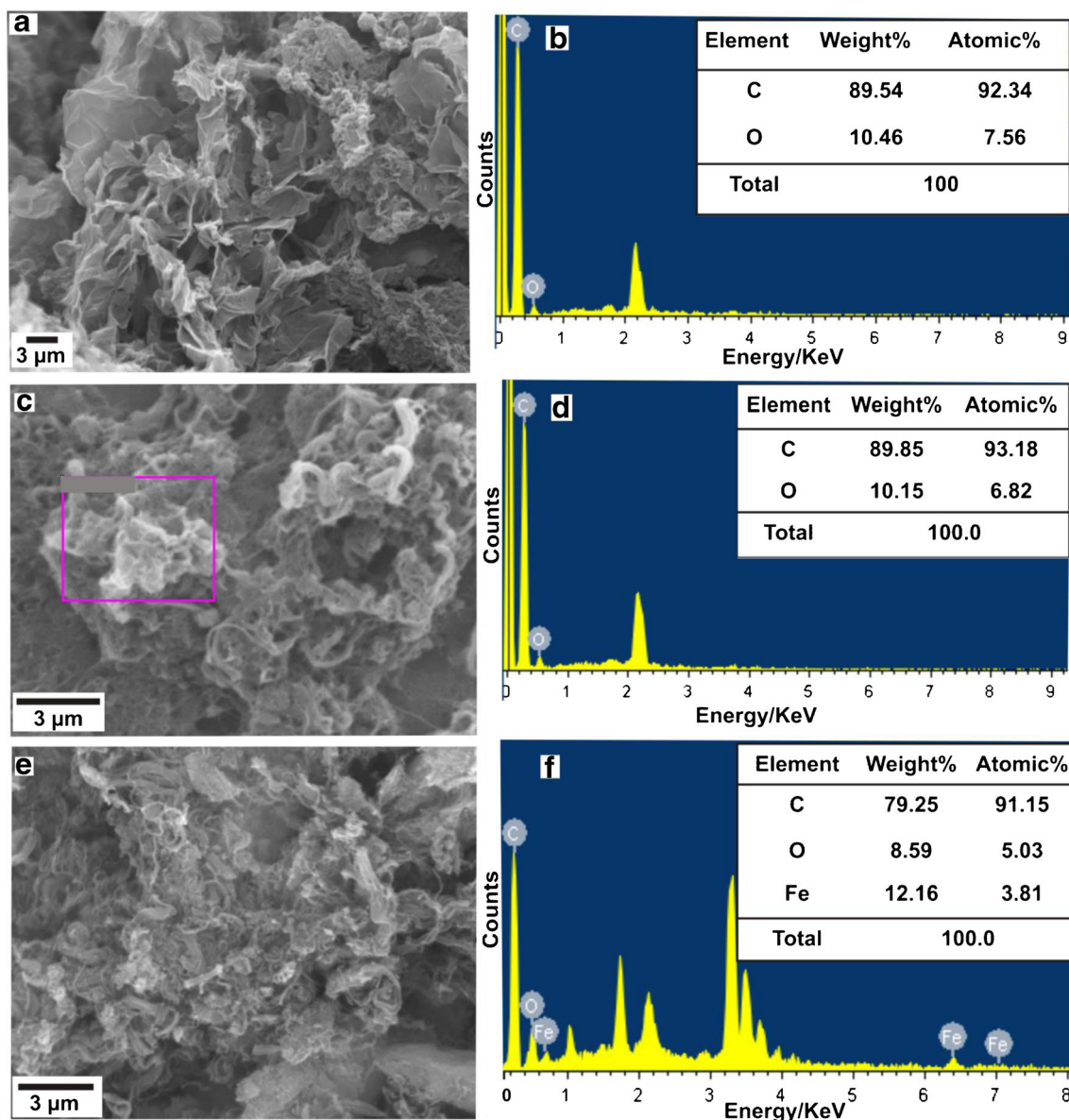


Fig. 1 SEM images of graphene (a), GR-MWCNTs hybrid (c), and GR-MWCNTs/FeNPs nanocomposite (e). EDX analysis of graphene (b), GR-MWCNTs hybrid (d), and GR-MWCNTs/FeNPs nanocomposite (f)

conducting properties of GR-MWCNTs hybrid film. Furthermore, EIS of GR-MWCNTs/FeNPs/GCE exhibited almost only the linear part indicated diffusion limited process revealed the superior electrical conductivity of the nanocomposite owing to the excellent synergy between GR, MWCNTs, and Fe nanoparticles.

Figure 3b displays the XRD patterns of GO (a), GR-MWCNTs hybrid (b), and GR-MWCNTs/FeNPs nanocomposite (c). XRD pattern of GO showed well defined and sharp diffraction peak (0 0 2) at 2θ of 11.3° corresponding to large interlayer d -spacing (8.02 Å) which confirmed the successful formation of GO. XRD pattern of GR-CNTs hybrid showed the presence of new diffraction peaks at 25.2° with disappearance of peak at 11.3° . The new diffraction peak appeared

at 25.2° (d -spacing of 0.349 nm) is the characteristic graphitic network of GR. Moreover, the disappearance of peak at 11.3° shows the successful reduction of GO to GR. XRD pattern of GR-MWCNTs/FeNPs possess a new diffraction peak at 44.01° , attributed to the successful formation of Fe nanoparticles (100) [27].

Investigation of nitrite oxidation by cyclic voltammetry

The influence of pH of the supporting electrolyte has been investigated to choose the optimum pH for the electrocatalytic experiments (inset to Fig. 4a). Cyclic voltammograms (CVs) were carried out at the GR-MWCNTs/FeNPs film-modified GCE in various buffer solutions (pH ranges from 1 to 9)

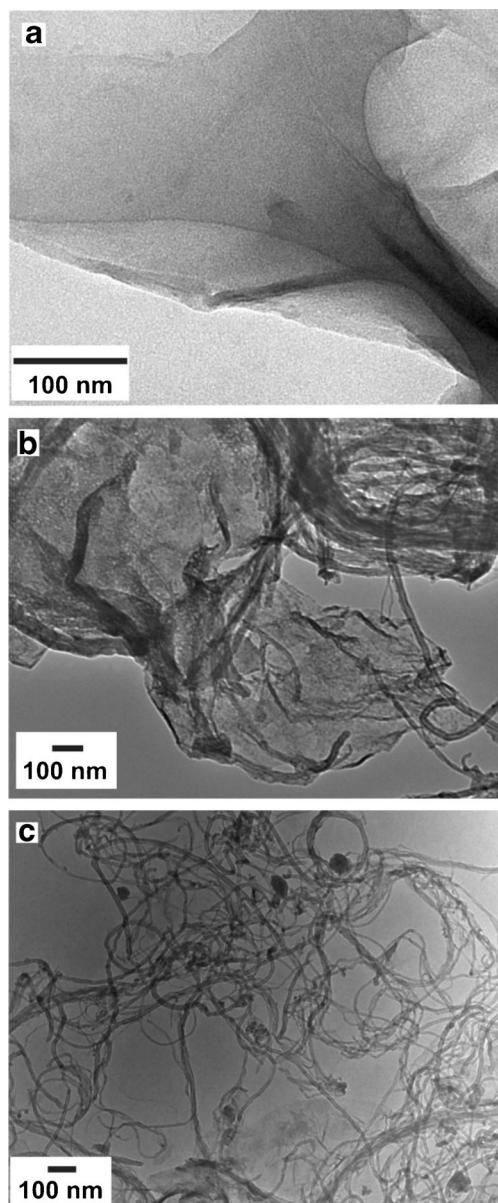


Fig. 2 TEM of graphene (a), GR-MWCNTs hybrid (b), and GR-MWCNTs/FeNPs nanocomposite (c)

towards electrocatalytic oxidation of 1-mM nitrite. As shown in the plot, nitrite oxidation peak current is significantly affected in different pH solutions. The oxidation peak current increases from pH of 1 to 5 and decreases from 5 to 9. When the pH of the supporting electrolyte is less than 5, the NO_2^- ions are unstable and hence, it can convert into NO and NO_3^- resulting in peak currents decrease. When the pH of the supporting electrolyte is greater than 5, the oxidation of nitrite becomes more difficult due to the shortage of protons and therefore the peak currents decrease. Since maximum electrocatalytic response is observed at the pH 5, we choose this pH for all the electrochemical experiments. Figure 4a shows the CVs obtained at bare (a), GR (b), MWCNTs (c), GR-MWCNTs (b) and GR-MWCNTs/FeNPs nanocomposite (c)

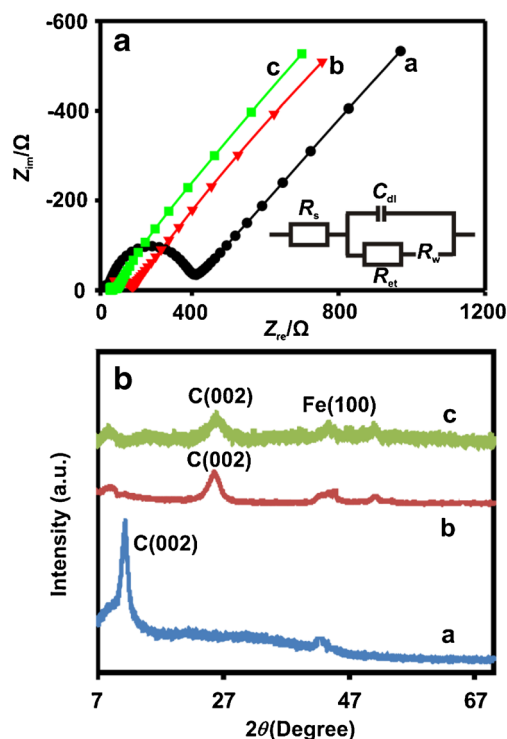


Fig. 3 a EIS of bare (a), GR-MWCNTs hybrid (b), GR-MWCNTs/FeNPs nanocomposite (c) film-modified GCEs in PBS (pH 7) containing 5 mM of $\text{Fe}(\text{CN})_6^{3-/4-}$. Bias potential=0 V, amplitude=5 mV, Frequency=0.1 to 100 kHz. b XRD patterns of GO (a) GR-MWCNTs hybrid (b) and GR-MWCNTs/FeNPs nanocomposite (c)

films modified GCEs in PBS (pH 5) towards 1-mM nitrite. Electro-oxidation peak of nitrite at the bare GCE and GR/GCE occurred at high overpotential +0.93 and +1.01 V. While both MWCNTs and GR-MWCNTs exhibited relatively less overpotential +0.80 V for the nitrite oxidation, whereas nitrite oxidation peak at the GR-MWCNTs/FeNPs/GCE exhibited lowest overpotential +0.77 mV than all the aforementioned electrodes. Notably, nitrite oxidation peak current (I_p) is 2.45-fold enhanced while peak potential is decreased by 210 mV at GR-MWCNTs/GCE than those at bare GCE. Likewise, 2.8-fold enhancement in I_p and 240-mV decrease in peak potential was observed at GR-MWCNTs/FeNPs/GCE than those at bare GCE. Thus, both GR-CNTs and GR-MWCNTs/FeNPs nanocomposite exhibited better electrocatalytic ability towards oxidation of nitrite than bare GCE in terms of both increase in peak currents and decrease in overpotential. In particular, GR-MWCNTs/FeNPs nanocomposite shows more enhanced I_p with 30-mV less positive potential when compared with GR-MWCNTs hybrid. This shows that incorporated Fe nanoparticles have its special role towards enhancing the electrocatalysis of nitrite oxidation. Accordingly, GR-MWCNTs/FeNPs/GCE has excellent electrocatalytic ability towards electro-oxidation of nitrite. Perhaps, there might be a great synergic effect between GR, MWCNTs, and FeNPs which facilitated the superior electrocatalytic performance of

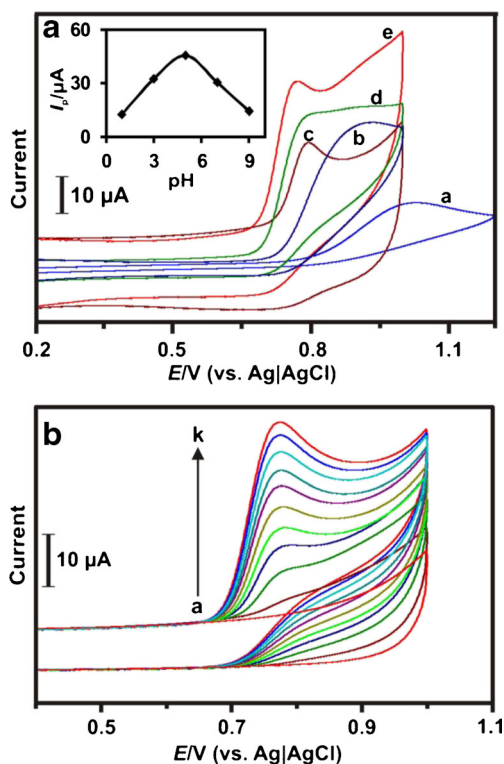


Fig. 4 **a** CVs at bare GCE (*a*), GR (*b*), MWCNTs (*c*), GR-MWCNTs hybrid (*d*), GR-MWCNTs/FeNPs nanocomposite (*e*) film-modified GCEs in PBS (pH 5) containing 1-mM of nitrite at the scan rate of 50 mVs^{-1} . **b** CVs of GR-MWCNTs/FeNPs/GCE in PBS (pH 5) in the presence of nitrite ranging from 0.1 to 1 mM (*a* to *j*)

the nanocomposite towards oxidation of nitrite than that of individual components.

Electrocatalysis of nitrite at GR-MWCNTs/FeNPs/GCE

Figure 4b shows the CVs of GR-MWCNTs/FeNPs/GCE obtained for the various concentrations of nitrite in PBS (pH 5) at the scan rate 50 mVs^{-1} . Nitrite oxidation peak current appeared at +770 mV increased linearly with increase in concentrations of nitrite from 0.1 to 1 mM. The observed linear increase in I_p with increase in concentrations of nitrite revealed the excellent electrocatalytic ability of the modified electrode towards electro-oxidation of nitrite. Therefore, we employed the GR-MWCNTs/FeNPs/GCE for the sensitive determination of nitrite via amperometry.

Figure 5 shows the CVs obtained at GR-MWCNTs/FeNPs/GCE for different scan rates (ν) from 0.1 to 1 Vs^{-1} in PBS (pH 5) containing 1-mM nitrite. I_p increased linearly with scan rates from 0.1 to 1 Vs^{-1} . Moreover, a plot of I_p versus $\nu^{1/2}$ (inset to Fig. 5) exhibited linear relationship indicated diffusion controlled process. The corresponding linear regression equation can be expressed as I_p (microampere) = $52.85 (\pm 0.08) \nu^{1/2} (\text{Vs}^{-1})^{1/2} + 1.67 (\pm 0.15)$, $R^2 = 0.985$. Moreover, the anodic peak potential (E_{pa}) shifts to higher positive potentials with the increase in scan rate. A plot of E_{pa} versus $\log \nu$ presume a

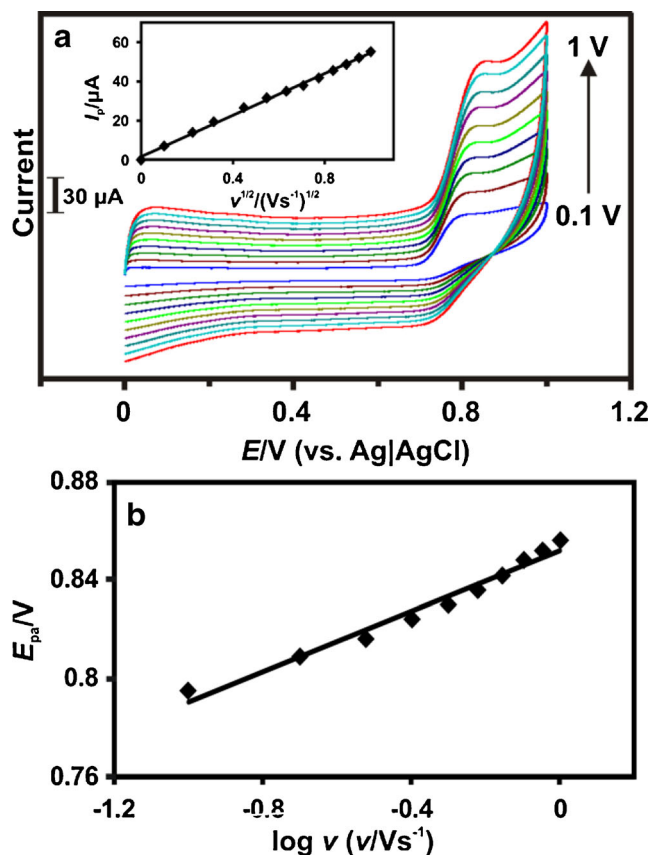


Fig. 5 **a** CVs of GR-MWCNTs/FeNPs/GCE at different scan rates from 0.1 to 1 Vs^{-1} in PBS (pH 5) containing 1-mM of nitrite. Inset plot of I_p versus $\nu^{1/2}$. **b** Plot of E_{pa} versus $\log \nu$

linear relationship and the linear regression equation can be expressed as, $E_{pa} (\text{V}) = 0.06 (\pm 0.02) \log \nu (\text{Vs}^{-1}) + 0.85 (\pm 0.09)$, $R^2 = 0.974$ (Fig. 5b). This result implies that electrocatalytic oxidation process of NO_2^- at the GR-MWCNTs/FeNPs/GCE is a chemically irreversible process. For an irreversible process, the electron transfer coefficient (α) and the number of electron transfer involved in the rate-determining step (n_a) can be related as Eq. (1),

$$E_{pa} = [2.303RT/2(1-\alpha)n_aF]\log \nu + K \quad (1)$$

Where, K is a constant and the other terms have their usual conventional meanings. By assuming n_a as 1 and substituting the slope of E_{pa} versus $\log \nu$ plot in the Eq. (1), the value of α can be obtained as $0.52 (\pm 0.05)$ for the nitrite oxidation. Further, the number of electrons (n) involved in the nitrite oxidation process is estimated from the slope of I_p versus $\nu^{1/2}$ plot and by using the Eq. (2) for the totally irreversible process controlled by diffusion [28].

$$I_p = (2.99 \times 10^5) n [(1-\alpha)n_a]^{1/2} A C_o * D_o^{1/2} \nu^{1/2} \quad (2)$$

In the above equation, D_o (square centimeter per second) is the diffusion coefficient of the nitrite ($2.1 \times 10^{-5} \text{ cm}^2 \text{ s}^{-1}$), A is

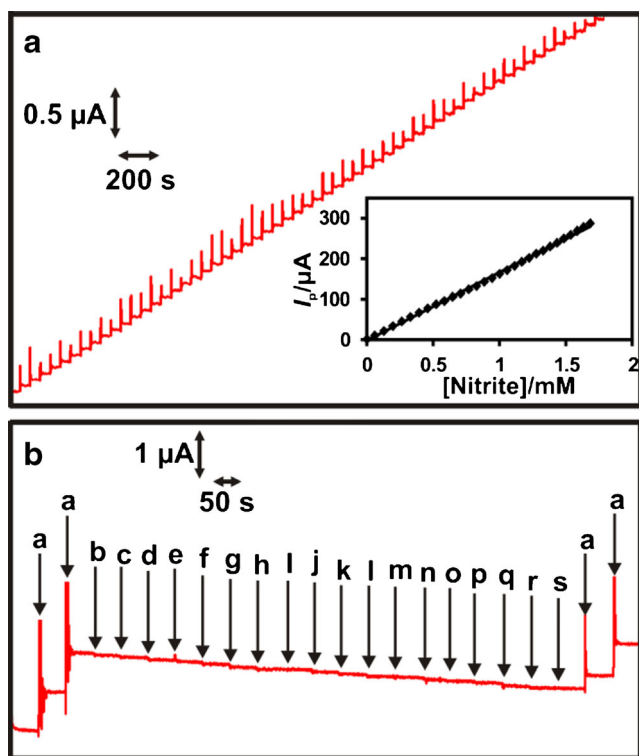
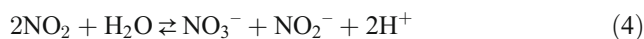


Fig. 6 **a** Amperometric *i*-*t* response obtained at GR-MWCNTs/FeNPs/RDE upon each successive additions of 1- μ M nitrite into continuously stirred PBS (pH 5). Rotation speed=1,500 rpm; E_{app} =+0.77 V. *Inset* calibration plot of [nitrite] versus I_p . **b** Amperometric *i*-*t* obtained at GR-MWCNTs/FeNPs/RDE upon each successive addition of 5- μ M NO_2^- (a) in the presence of 250-fold excess of F^- (b), Cl^- (c), Br^- (d), I^- (e), NO_3^- (f) and NH_4^+ (g), each 100-fold excess of Na^+ (h), K^+ (i), glucose (j), sucrose (k), and urea (l) and each 40-fold excess of Mg^{2+} (m), Ca^{2+} (n), Ba^{2+} (o), Ni^{2+} (p), oxalate (q), SO_4^{2-} (r), and CO_3^{2-} (s) into continuously stirred PBS (pH 5)

the electrode area, C_o^* (mole per cubic centimeter) is the bulk concentration of nitrite and the other parameters have their

conventional meanings. By substituting all the values in Eq. (2), the value of *n* has been estimated to be about 2. This indicates that NO_3^- is the only possible final product in the nitrite oxidation reaction which is also in good accordance with the literature and the possible mechanism can be expressed as formation of NO_2 as a first step, followed by a disproportionate reaction of NO_2 and the overall reaction process can be expressed by Eqs. (3) and (4) [28, 29].



Amperometric determination of nitrite

Figure 6a shows the amperogram obtained at GR-MWCNTs/FeNPs/RDE at the rotation speed of 1,500 RPM towards each sequential additions of nitrite (each 1 μ M) for every 50 s into continuously stirred PBS (pH 5). Applied potential (E_{app}) was held at +0.77 V. For every addition of nitrite, a quick and stable amperometric response was observed and the respective amperometric response currents increased linearly in the concentration range of 1×10^{-7} M to 1.68×10^{-3} M.

A calibration plot was made between [nitrite] versus I_p (Inset to Fig. 6a) and the respective linear regression equation was expressed as I_p (microampere)=0.17 (± 0.07) [nitrite] (microampere) - 0.938 (± 1.1), $R^2=0.998$. Sensitivity and detection limit (LOD) of the sensor were calculated to be 0.70 (± 0.04) $\mu\text{A } \mu\text{M}^{-1} \text{ cm}^{-2}$ and 75.6 (± 1.3) nM, respectively. Excellent performance of the GR-MWCNTs/FeNPs

Table 1 Comparison of electroanalytical parameters for the determination nitrite at the GR-MWCNTs/FeNPs/GCE with various modified electrodes

Electrode	Potential (V)	Linear range (μM)	LOD (μM)	Sensitivity	Ref.
Au nanoparticles-sulfonated graphene composite	+0.73 (versus SCE)	10–3,960	0.2	0.045 $\mu\text{A } \mu\text{M}^{-1}$	[20]
Reduced graphene oxide–MWCNTs	+0.80 (versus SCE)	75–6,060	25	NA	[21]
Bare GCE	+0.80 (versus SCE)	2.5–10	0.4	36 mA M^{-1}	[22]
Graphene/polypyrrole/chitosan nanocomposite	+0.90 (versus SCE)	0.5–722	0.1	NA	[23]
Reduced graphene oxide	+0.80 (versus Ag AgCl, sat. KCl)	8.9–167	1	0.027 $\mu\text{A } \mu\text{M}^{-1} \text{ cm}^{-2}$	[24]
Thionine/aligned CNTs	+0.80 (versus Ag AgCl, sat. KCl)	3–500	1.12	NA	[25]
Nano alumina	+0.80 (versus SCE)	0.05–1100	0.01	NA	[30]
poly(toluidine blue)	+1.10 (versus SCE)	0.1–15.2	0.05	0.47 $\mu\text{A } \mu\text{M}^{-1} \text{ cm}^{-2}$	[31]
Cytochrome c/DNA/MWCNT-poly(amidoamine)-Chitosan	+0.95 (versus SCE)	0.2–80	0.03	NA	[32]
GR-MWCNTs/FeNPs nanocomposite	+0.77 (versus Ag AgCl, sat. KCl)	0.1–1680	0.076 (± 1.3)	0.697 $\mu\text{A } \mu\text{M}^{-1} \text{ cm}^{-2}$	This work

LOD limit of detection, SCE standard calomel electrode, NA not available

nanocomposite film-modified electrode based sensor towards the determination of nitrite has been assessed by the exceptional analytical parameters achieved such as low LOD, high sensitivity, and wide linear range. The important analytical parameters obtained at the GR-MWCNTs/FeNPs/GCE were compared other nitrite sensors (Table 1). As can be seen from Table 1, the analytical performances of the proposed sensor were quit comparable to the performances of the previously reported nitrite sensors.

Interference studies

We investigated the selectivity of the proposed sensor towards nitrite detection in the presence of common ions such as F^- , Cl^- , Br^- , I^- , Na^+ , K^+ , Mg^{2+} , Ca^{2+} , Ba^{2+} , NH_4^+ , Ni^{2+} , NO_3^- , SO_4^{2-} , CO_3^{2-} , and biological interferences such as glucose, sucrose, oxalate, and urea. The experimental conditions are same as Fig. 6a and the respective amperogram is shown in Fig. 6b. The sensor exhibited quick and well defined amperometric response towards each addition of 5- μ M NO_2^- (a), whereas, no noteworthy responses were observed upon each 250-fold excess of F^- (b), Cl^- (c), Br^- (d), I^- (e), NO_3^- (f) and NH_4^+ (g), each 100-fold excess of Na^+ (h), K^+ (i), glucose (j), sucrose (k), and urea (l) and 40-fold excess of Mg^{2+} (m), Ca^{2+} (n), Ba^{2+} (o), Ni^{2+} (p), oxalate (q), SO_4^{2-} (r), and CO_3^{2-} (s). However, notable amperometric response was obtained immediately upon addition of 5- μ M NO_2^- into the above mentioned interferences coexisted PBS revealing the excellent selectivity of the sensor for the determination of nitrite. Thus, the GR-MWCNTs/FeNPs/GCE able to detect nitrite selectively even in the presence of excess concentration of common interfering ions and biological interferences.

Determination of nitrite in various water samples

Practical feasibility of the proposed sensor has been demonstrated by the determination of nitrite in various water samples collected from different water sources such as river, tap, and rain. Known amounts of nitrite were spiked into the water samples and analyzed using GR-MWCNTs/FeNPs film-modified electrode by amperometry. Standard addition method was adopted to find the recoveries and the respective results were given as Table 2. The added and found values showed good recoveries from 96.1 to 103.7 % revealed the appreciable practicality of the proposed sensor.

Repeatability, reproducibility, and stability studies

Repeatability and reproducibility of the sensor towards determination of nitrite has been evaluated by CV studies.

Table 2 Determination of nitrite in spiked water samples at the GR-MWCNTs/FeNPs/GCE

Samples	Added (μ M)	Found (μ M)	Recovery (%)	RSD (%) ^a
River water	5	5.05	101	2.8
	10	10.28	102.8	3.6
Tap water	5	4.86	97.2	3.1
	10	10.37	103.7	2.3
Rain water	5	4.81	98.37	3.8
	10	9.61	96.1	3.2

^a Relative standard deviation of three individual measurements

CVs were recorded in PBS (pH 5) towards electrocatalytic determination of 1-mM nitrite. The results showed that the sensor exhibited good repeatability with relative standard deviation (R.S.D) of 3.55 % for eight successive repetitive measurements. Similarly, the modified electrode exhibited good reproducibility with R.S.D of 2.52 % for four individual measurements at the same modified electrode. In order to determine the storage stability, GR-MWCNTs/FeNPs/GCE was stored in PBS at 4 °C and I_p towards 1-mM nitrite have been recorded everyday by CV. The modified electrode retained 94.3 % of its initial I_p even after 3 weeks of its storage validated good storage stability. Moreover, we investigated the operational stability of the modified electrode under hydrodynamic conditions. Only 6 % of I_p was decreased even after continuous rotating for 4,000 s, representing excellent operational stability of the modified electrode. Thus, both storage and operational stabilities are appreciable attributed to the good adhesion and high stability of the GR-MWCNTs/FeNPs nanocomposite film.

Conclusions

We successfully prepared and characterized GR-MWCNTs/FeNPs nanocomposite and employed it for the sensitive determination of nitrite. CV results proved that oxidation of nitrite is highly efficient at the GR-MWCNTs/FeNPs in terms of significant enhancement in I_p and decrease in overpotential. The fabricated amperometric sensor exhibited excellent analytical parameters with wide linear range, high sensitivity, and notably, very low LOD of 75.6 (\pm 1.3)nM. The sensor is highly selective towards determination of nitrite even in the presence of large quantity of common ions and biological interferences. Moreover, the sensor shows good recovery results in the real sample studies revealed its excellent practicality. Furthermore, the sensor offered appreciable repeatability, reproducibility and stability results.

Acknowledgment This work was supported by the National Science Council and the Ministry of Education of Taiwan (Republic of China).

References

- Shao Y, Wang J, Wu H, Liu J, Aksay IA, Lin Y (2010) Graphene based electrochemical sensors and biosensors: a review. *Electroanalysis* 22:1027–1036
- Soldano C, Mahmood A, Dujardin E (2010) Production, properties and potential of graphene. *Carbon* 48:2127–2150
- Novoselov KS, Geim AK, Morozov SV, Jiang D, Zhang Y, Dubonos SV, Grigorieva IV, Firsov AA (2004) Electric field effect in atomically thin carbon films. *Science* 306:666–669
- Lopez BP, Merkoci A (2012) Carbon nanotubes and graphene in analytical sciences. *Microchim Acta* 179:1–16
- Pumera M, Ambrosi A, Bonanni A, Chng ELK, Poh HL (2010) Graphene for electrochemical sensing and biosensing. *TrAC Trends Anal Chem* 29:954–965
- Woo S, Kim YR, Chung TD, Piao Y, Kim H (2012) Synthesis of graphene–carbon nanotubes composite and its electrochemical sensing of hydrogen peroxide. *Electrochim Acta* 59:509–514
- Sasikaladevi S, Aravind J, Eswaraiah V, Ramaprabhu S (2011) Facile synthesis of one dimensional graphene wrapped carbon nanotubes composites by chemical vapour deposition. *J Mater Chem* 21:15179–15182
- Yu D, Dai L (2010) Self-assembled graphene/carbon nanotube hybrid films for supercapacitors. *J Phys Chem Lett* 1:467–470
- Yen MY, Hsiao MC, Liao SH, Liu PI, Tsai HM, Ma CCM, Pu NW, Ger MD (2011) Preparation of graphene/multi-walled carbon nanotube hybrid and its use as photoanodes of dye-sensitized solar cells. *Carbon* 49:3597–3606
- Unnikrishnan B, Mani V, Chen SM (2012) Highly sensitive amperometric sensor for carbamazepine determination based on electrochemically reduced graphene oxide-single-walled carbon nanotubes composite film. *Sens Actuators B* 173:274–280
- Mani V, Devadas B, Chen SM (2013) Direct electrochemistry of glucose oxidase at electrochemically reduced graphene oxide-multiwalled carbon nanotubes hybrid material modified electrode for glucose biosensor. *Biosens Bioelectron* 41:309–315
- Du HY, Wang CH, Hsu HC, Chang ST, Huang HC, Chen LC, Chen KH (2012) Graphene nanosheet–CNT hybrid nanostructure electrode for a proton exchange membrane fuel cell. *Int J Hydrog Energy* 37:18989–18995
- Stoner BR, Glass JT (2012) Carbon nanostructures: a morphological classification for charge density optimization. *Diamond Relat Mater* 23:130–134
- Buglione L, Pumera M (2012) Graphene/carbon nanotube composites not exhibiting synergic effect for supercapacitors: the resulting capacitance being average of capacitance of individual components. *Electrochem Commun* 17:45–47
- Wang Y, Wu Y, Huang Y, Zhang F, Yang X, Ma Y, Chen Y (2011) Preventing graphene sheets from restacking for high-capacitance performance. *J Phys Chem C* 115:23192–23197
- Atta NF, Ahmed RA, Amin HMA, Galal A (2012) Monodispersed gold nanoparticles decorated carbon nanotubes as an enhanced sensing platform for nanomolar detection of tramadol. *Electroanalysis* 24: 2135–2146
- Xu C, Wang X, Zhu J (2008) Graphene-metal particle nanocomposites. *J Phys Chem C* 112:19841–19845
- Aravind SSJ, Ramaprabhu S (2012) Pt nanoparticle-dispersed graphene-wrapped MWNT composites as oxygen reduction reaction electrocatalyst in proton exchange membrane fuel cell. *ACS Appl Mater Interfaces* 4:3805–3810
- Liu TS, Kang TF, Lu LP, Zhang Y, Cheng SY (2009) Au–Fe(III) nanoparticle modified glassy carbon electrode for electrochemical nitrite sensor. *J Electroanal Chem* 632:197–200
- Li SJ, Zhao GY, Zhang RX, Hou YL, Liu L, Pang H (2013) A sensitive and selective nitrite sensor based on a glassy carbon electrode modified with gold nanoparticles and sulfonated graphene. *Microchim Acta* 180:821–827
- Hu F, Chen S, Wang C, Yuan R, Yuan D, Wang C (2012) Study on the application of reduced graphene oxide and multiwall carbon nanotubes hybrid materials for simultaneous determination of catechol, hydroquinone, p-cresol and nitrite. *Anal Chim Acta* 724:40–46
- Kozub BR, Rees NV, Compton RG (2010) Electrochemical determination of nitrite at a bare glassy carbon electrode; why chemically modify electrodes? *Sens Actuators B* 143:539–546
- Ye D, Luo L, Ding Y, Chen Q, Liu X (2011) A novel nitrite sensor based on graphene/polypyrrole/chitosan nanocomposite modified glassy carbon electrode. *Analyst* 136:4563–4569
- Mani V, Periasamy AP, Chen SM (2012) Highly selective amperometric nitrite sensor based on chemically reduced graphene oxide modified electrode. *Electrochem Commun* 17:75–78
- Zhao K, Song H, Zhuang S, Dai L, He P, Fang Y (2007) Determination of nitrite with the electrocatalytic property to the oxidation of nitrite on thionine modified aligned carbon nanotubes. *Electrochem Commun* 9:65–70
- Hummers WS, Offeman RE (1958) Preparation of graphitic oxide. *J Am Chem Soc* 80:1339
- Kassaei MZ, Motamedi E, Mikhak A, Rahnamaie R (2011) Nitrate removal from water using iron nanoparticles produced by arc discharge versus reduction. *Chem Eng J* 166:490–495
- Lin CY, Balamurugan A, Lai YH, Ho KC (2010) A novel poly(3,4-ethylenedioxythiophene)/iron phthalocyanine/multi-wall carbon nanotubes nanocomposite with high electrocatalytic activity for nitrite oxidation. *Talanta* 82:1905–1911
- Guidelli G, Pergola F, Raspi G (1972) Voltammetric behavior of nitrite ion on platinum in neutral and weakly acidic media. *Anal Chem* 44:745–755
- He Q, Gan T, Zheng D, Hu S (2010) Direct electrochemistry and electrocatalysis of nitrite based on nano-alumina-modified electrode. *J Solid State Electrochem* 14:1057–1064
- Yang C, Xu J, Hu S (2007) Development of a novel nitrite amperometric sensor based on poly(toluidine blue) film electrode. *J Solid State Electrochem* 11:514–520
- Chen Q, Ai S, Fan H, Cai J, Ma Q, Zhu X, Yin H (2010) The immobilization of Cytochrome c on MWNT–PAMAM–Chit nanocomposite incorporated with DNA biocomposite film modified glassy carbon electrode for the determination of nitrite. *J Solid State Electrochem* 14:1681–1688